REPORT DOCUMENTATION PAGE

Form Approved OMB NO. 0704-0188

1. REPORT DATE (DD-MM-YYYY)	2. REPORT TYPE	3. DATES COVERED (From - To)
06-07-2021	Final Report	27-Sep-2017 - 31-Mar-2021

4. TITLE AND SUBTITLE
Final Report: Topological Photonic Line Waveguides for High Performance Optoelectronic Devices

5a. CONTRACT NUMBER
W911NF-17-1-0580

5b. GRANT NUMBER

5c. PROGRAM ELEMENT NUMBER

6. AUTHORS

5d. PROJECT NUMBER

5e. TASK NUMBER

5f. WORK UNIT NUMBER

7. PERFORMING ORGANIZATION NAMES AND ADDRESSES
University of California - San Diego
Office of Contract & Grant Adm
9500 Gilman drive, MC 0934
La Jolla, CA 92093 -0934

8. PERFORMING ORGANIZATION REPORT NUMBER

9. SPONSORING/MONITORING AGENCY NAME(S) AND ADDRESS (ES)
U.S. Army Research Office
P.O. Box 12211
Research Triangle Park, NC 27709-2211

10. SPONSOR/MONITOR'S ACRONYM(S)
ARO

11. SPONSOR/MONITOR'S REPORT NUMBER(S)
72310-EL-DRP.2

12. DISTRIBUTION AVAILIBILITY STATEMENT
Approved for public release; distribution is unlimited.

13. SUPPLEMENTARY NOTES
The views, opinions and/or findings contained in this report are those of the author(s) and should not contrued as an official Department of the Army position, policy or decision, unless so designated by other documentation.

14. ABSTRACT

15. SUBJECT TERMS

16. SECURITY CLASSIFICATION OF:			17. LIMITATION OF ABSTRACT	15. NUMBER OF PAGES	19a. NAME OF RESPONSIBLE PERSON
a. REPORT	b. ABSTRACT	c. THIS PAGE			Daniel Sievenpiper
UU	UU	UU	UU		19b. TELEPHONE NUMBER 858-822-6678

RPPR Final Report
as of 14-Jul-2021

Agency Code: 21XD

Proposal Number: 72310ELDRP **Agreement Number: W911NF-17-1-0580**
INVESTIGATOR(S):

Name: Daniel Sievenpiper
Email: DSIEVENPIPER@UCSD.EDU
Phone Number: 8588226678
Principal: Y

Organization: **University of California - San Diego**
Address: Office of Contract & Grant Adm, La Jolla, CA 920930934
Country: USA
DUNS Number: 804355790 EIN: 956006144

Report Date: 30-Jun-2021 Date Received: 06-Jul-2021
Final Report for Period Beginning 27-Sep-2017 and Ending 31-Mar-2021
Title: Topological Photonic Line Waveguides for High Performance Optoelectronic Devices
Begin Performance Period: 27-Sep-2017 **End Performance Period:** 31-Mar-2021
Report Term: 0-Other

Submitted By: Daniel Sievenpiper Email: DSIEVENPIPER@UCSD.EDU
Phone: (858) 822-6678

Distribution Statement: 1-Approved for public release; distribution is unlimited.

STEM Degrees: 0 **STEM Participants:** 1

Major Goals: The primary goal of this program is to develop photonic “line waves”, or photonic topological insulators that can be made into practical structures for photonic integrated waveguides and devices. The concept of “line waves" has been recently developed at microwave frequencies, and these waves have been shown to achieve unidirectional propagation, thereby being highly resistant to backscattering. This can potentially solve the scattering problem that is common to photonic integrated circuits. The goal of this work is to develop existing line wave structures into new versions that are practical for optical frequencies, preferably eliminating the need for metallic components, and then to implement them on a practical photonic platform to demonstrate their capabilities.

Accomplishments: During the previous reporting period, we successfully fabricated optical structures and measured them. We initially ran into difficulty fabricating these devices on campus due to the limitations imposed by the Covid lockdowns. However, we were able to identify a third-party vendor who could build and test our designs for us. We fabricated waveguides with sharp turns, zigzag structures, and magic-T junctions. We also fabricated conventional photonic crystal waveguides as a reference. We were able to show that the topological waveguides achieved significantly better performance than the photonic crystal waveguides and achieved low loss even after several sharp bends. The magic-T structure also worked as expected. During this reporting period, we have not been doing any technical work as that is essentially finished. We have been writing and submitting a manuscript on this work for publication.

Training Opportunities: Nothing to Report

Results Dissemination: We have been working on getting our manuscript published to publicize our primary results in this program, which are our successful optical measurements. This effort is still ongoing.

Honors and Awards: Nothing to Report

Protocol Activity Status:

Technology Transfer: Nothing to Report

PARTICIPANTS:

Participant Type: Graduate Student (research assistant)

RPPR Final Report
as of 14-Jul-2021

Participant: Shreya Singh
Person Months Worked: 1.00 **Funding Support:**
Project Contribution:
National Academy Member: N

ARTICLES:

Publication Type: Journal Article Peer Reviewed: Y **Publication Status:** 1-Published
Journal: Laser & Photonics Reviews
Publication Identifier Type: DOI Publication Identifier: 10.1002/lpor.201900126
Volume: Issue: First Page #: 1900126
Date Submitted: 8/27/19 12:00AM Date Published: 8/1/19 7:00AM
Publication Location:
Article Title: Electromagnetic?Dual Metasurfaces for Topological States along a 1D Interface
Authors: Dia'aaldin J. Bisharat, Daniel F. Sievenpiper
Keywords: photonic topological insulator, metasurface
Abstract: The discovery of topological insulators was rapidly followed by the advent of their photonic analogues, motivated by the prospect of backscattering- immune light propagation. So far, however, implementations have mainly relied on engineering bulk modes in photonic crystals and waveguide arrays in two- dimensional (2D) systems, which closely mimic their electronic counterparts. In addition, metamaterials-based implementations subject to electromagnetic duality and bianisotropy conditions suffer from intricate designs and narrow operating bandwidths. Here, it is shown that symmetry-protected topological states akin to the quantum spin-Hall effect can be realized in a straightforward manner by coupling surface modes over metasurfaces of complementary electromagnetic responses. Specifically, stacking unit cells of such metasurfaces directly results in double Dirac cones of degenerate transverse- electric (TE) and transverse-magnetic (TM) modes, which break into a wide nontrivial bandgap at
Distribution Statement: 3-Distribution authorized to U.S. Government Agencies and their contractors
Acknowledged Federal Support: **Y**

Partners

,

I certify that the information in the report is complete and accurate:
Signature: Dan Sievenpiper
Signature Date: 7/6/21 7:23PM

Local valley Hall effect for robust transport beyond topology

Dia'aaldin J. Bisharat & Daniel F. Sievenpiper

Electrical and Computer Engineering Department, University of California San Diego, La Jolla, CA 92093, USA

Abstract: Valley-contrast physics has gained considerable attention, particularly in designing quantum valley Hall effect-type photonic topological insulators (PTIs). These structures host propagating valley-polarized modes at their edge that are reflection-free in the absence of inter-valley scattering defects, making them robust against zigzag bends. It is an open question whether similar robust states can exist in the absence of topological order. Here we present a new paradigm, coined the local valley Hall effect, to support valley polarized edge modes using triangular (C_{6v} symmetric) lattice photonic crystal (PhC), wherein the topological valley phase vanishes. We create a waveguide interface by breaking mirror inversion symmetry locally (i.e. only near the interface) using a line defect in the bulk, thus giving rise to locked orbital angular momentum states like in conventional valley PTIs but without requiring two distinct PhCs (topological domains). We fabricate our device on a silicon-on-insulator slab and characterize it at near-infrared frequencies showing similar transmission results along straight and sharply bent pathways over a broad bandwidth –indistinguishable from those of valley PTIs. Our results reveal the role of interface effects in forming backscattering-immune edge modes and, for the first time, put forward an alternative, simpler approach than current PTIs for realizing compact integrated photonic devices with little to no loss, thus benefiting practical applications and nanofabrication.

Introduction: There is a great need to employ photons in lieu of electrons in microchips currently used for transmitting data. Photonic systems promise to be faster and to deliver high data rates all while saving energy. While applications such as on-chip photonic communication are already in use, a major drawback of the current technology is that such systems cannot turn light efficiently, hence such devices have large footprint. This makes routing light around sharp corners in microscopic spaces while minimizing losses a necessity. Until recently, this feat was generally believed to be impossible except for only extremely narrow bands through an arduous optimization process of fine tune parameters that are unforgiving to fabrication errors. This conventional wisdom has been overturned with the advent of photonic topological insulators (PTIs) [1–20]. Just like their electronic counterparts, PTIs enable reflection-free propagation of edge modes along almost arbitrarily shaped interfaces separating two topologically distinct domains (i.e. bulks with different topological indices). The three basic topological phases – quantum Hall (QH) [4–6], quantum spin-Hall (QSH) [7–13], and quantum valley-Hall (QVH) [14–23] topological insulators– have all been emulated in photonics. Their implementations vary from gyromagnetic media [4–6], 3D chiral structures [7], bianisotropic metamaterials [8–10], array of coupled ring resonator [11] to all-dielectric structures with special crystalline symmetries [12–23]. The latter, which relies on the valley degree of freedom (DOF) in photonic crystals (PhCs), is of the most interest to the development of on-chip optical devices and is the motivation of this work.

The present study explores an example of 2D PhCs in which valley polarized propagation occurs like in the QVH case even though spatial-inversion symmetry (SIS) is present and the relevant topological index is zero. Generally, it is assumed that a valley-contrast response requires a transition to a topological valley phase, and so a reduction of the lattice symmetry. In addition,

valley polarized modes have only been observed at the edge between valley PTIs with opposite valley Chern numbers. Here we assess the degree to which these caveats are practically important. We present a new concept, coined local valley Hall effect (VHE), where the valley polarization is locally defined as opposed to being fixed throughout the bulk. Furthermore, we show how this enables us to create a line defect-type waveguide that supports direction-locked propagation immune to inter-valley scattering despite having identical PhCs (domains) across the waveguide interface. We validate our findings experimentally using a silicon-on-insulator (SOI) platform at telecommunication wavelengths and compare our device performance to that of a conventional valley PTI in case of straight and zigzag waveguide pathways, thus proving the efficacy of our approach.

Local VHE design:

We consider an all-dielectric 2D PhC slab with a triangular lattice of circular holes as shown in Fig. 1a. The band structure is plotted in Fig. 1e, which shows a bandgap for TE modes spanning a frequency range from the K point at the lower band to the M point at the higher band. Since the bandgap resides below the light cone, this ensures high–efficient light confinement in the plane of a chip and low out-of-plane radiation. Consequently, such configuration is widely used for PhC waveguides. The dashed line hexagons illustrate the Wigner–Seitz unit cell of the lattice; all hexagons are valid definitions of the unit cell and reproduce the same lattice. The unit cell that is centered at the hole (outlined in red in Fig. 1a) clearly preserves a mirror symmetry along ΓK direction. The two valleys, K and K', that sit at opposite corners (high-symmetry points) of the Brillouin zone (BZ) are well defined in the C_{6v} symmetric lattice by virtue of their large

separation in momentum space. The surface phase distribution map of the out-of-plane (vertical) magnetic field (H_z) at the extrema of band 1 coinciding with the K point is plotted in Fig. 1b. Numerical full-wave simulations show opposite orbital angular momentum (OAM) states that are evenly distributed throughout the bulk. Fig. 1c schematic illustrates a simplified color map of the same results. OAM states correspond to phase singular points, around which the phase incrementally increases, and their sign is determined by their clockwise/counter-clockwise rotation direction. Fig. 1d also plots the polarization of the in-plane (tangential) electric field, where the polarization ellipse is defined as ellipticity angles, $\chi = \arcsin\left[2|E_x||E_y|\sin\delta / (|E_x|^2 + |E_y|^2)\right]/2$, where $\delta=\delta_y-\delta_x$ is the phase difference between E_y and E_x. We find that right and left circular polarization (RCP, LCP) responses ($\chi=\pi/4$, $\chi=-\pi/4$) are distributed evenly through the PhC.

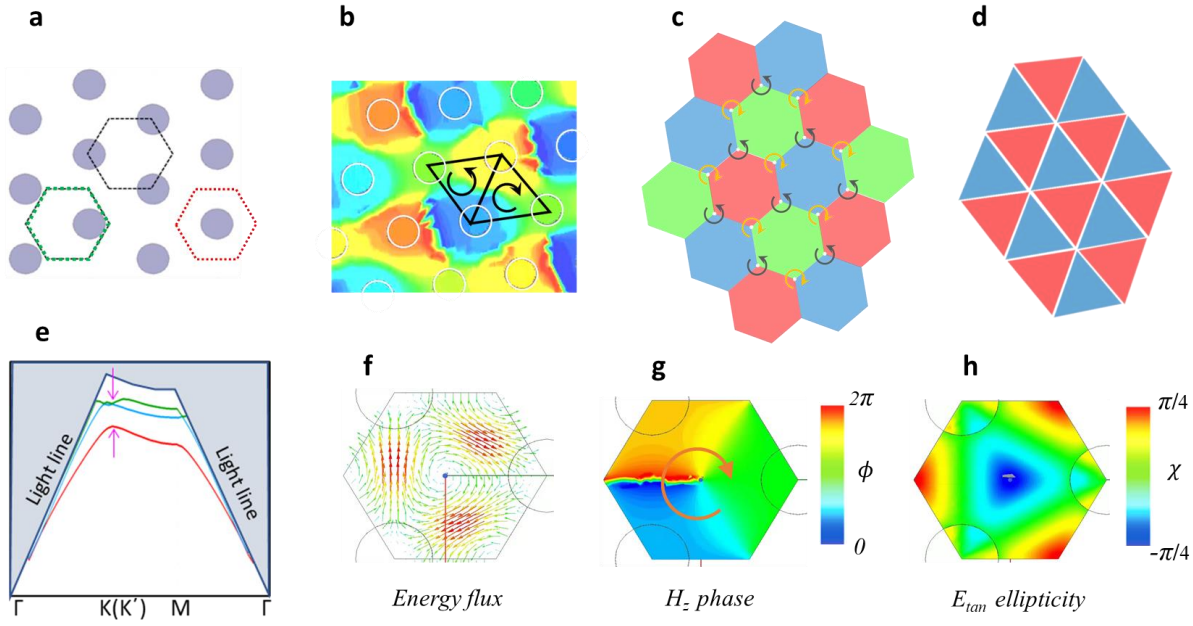

Figure 1. (a) Triangular lattice of air-holes in finite SOI and (e) the associated band diagram shows bandgap at K/K′ points. (b). Due to its high symmetry, this type of lattice does not -globally- qualify as valley PhC. One, however, notices that certain definitions of the unit cell resemble the asymmetric arrangement of air holes in valley PhCs, that is with the small air-hole being deleted. (c) Simulated phase vortex of H_z field profile and (d) ellipticity angle of (Ex, Ey) field at the K valley of the first band. (f)

plots of Poynting vector showing energy flux vortex at K valley. (g) Plot of the associated H_z phase showing phase singular point, which defines an OAM state. The phase winds up around the unit cell center either clockwise or counter-clockwise, depending on the definition of the unit cell (e.g., hexagon outlined in black in Fig. 1a). (h) Plot of the ellipticity angle of in-plane electric fields showing RCP response at the center of the unit cell. Meanwhile, LCP (red colors) response is observed at the corner of the unit cell.

Fig. 1f plots the energy flux, where the arrows represent the time-averaged Poynting vectors, of the first band at the K valley and show a mode profile that is invariant under 120° rotation. The center of the energy flux vortex corresponds to a phase singular point of H_z field (i.e. OAM state). As Fig. 1g shows, the associated phase profile winds clockwise by 2π phase around the center of the unit cell (note the unit cell is chosen such that holes are at the corners). Fig. 1h also shows a corresponding LCP response ($\chi=-\pi/4$) at the center of the unit cell at the K valley. Note that the field maps show opposite sign of OAM and CP fields located the corner of the unit cells. Therefore, if the unit cell is defined such that the three holes have the opposite orientation (mirror inverted, see black hexagon in Fig. 1a), the opposite sense of OAM and CP would be at the center of that unit cell. The fields at the K′ valley could be obtained by applying time-reversal operation, which reverses the direction of the energy flux and the phase rotation, and hence the sign of the OAM and CP states.

It is understood that photonic valley DOF in linked to OAM (and by extension CP) states, similar to the valley DOF in electronic systems, where the angular rotation of the electron wavefunction in the K or K' valleys of the band structure generates an intrinsic magnetic moment [24] analogous to that produced by the electron spin. Generally, SIS is broken to generate opposite, nonvanishing Berry curvature profiles near the K and K′ valleys which drives the anomalous transverse velocity, leading to VHE and topological valley phase [25]. Here we relax this restriction and establish, essentially, a more general, local version of the VHE. The hallmark of

this effect is that the valley polarization is locally defined as opposed to being fixed throughout the bulk. This is corroborated by the fact that OAM states are evenly present throughout our C_{6v} lattice as shown in Fig. 1, whereas a transition to topological valley phase, achieved via reduction to C_{3v} symmetry, promotes only one OAM state. The C_{6v} symmetry doubly preserves a three-fold rotation symmetry (C_{3v}), hence the associated mode profiles are necessarily purely CP at the high-symmetry points. Additionally, it follows that our PhC carries both signs of CP/OAM states at each valley, as discussed above.

Valley selective coupling:

Next, we show that valley-contrast response is possible in the triangular PhC without requiring a transition to a topological valley phase. We achieve selective excitation of valley-polarized states by exploiting the local VHE, that is the location dependence of the OAM state for each valley. This manifest in whether a specific OAM state is located at the center of the corner of a given unit cell. Accordingly, we infer that for a given location in the bulk, the K valley should exhibit opposite characteristic (OAM state) than the K' valley, which follows directly from time-reversal symmetry requirement. To observe that, we deign a finite area of the PhC with a hexagonal shaped boundary and place an external OAM source at the center of the PhC in the position marked A, as shown in Fig. 2a. Fig. 2b depicts a circular arrangement of a group of H_z dipole-point sources with same magnitudes but incrementally increasing phases used for generating OAM of different signs. The boundaries of the hexagon region are cut such that vertices are located along the ΓK and ΓK′ directions of the lattice.

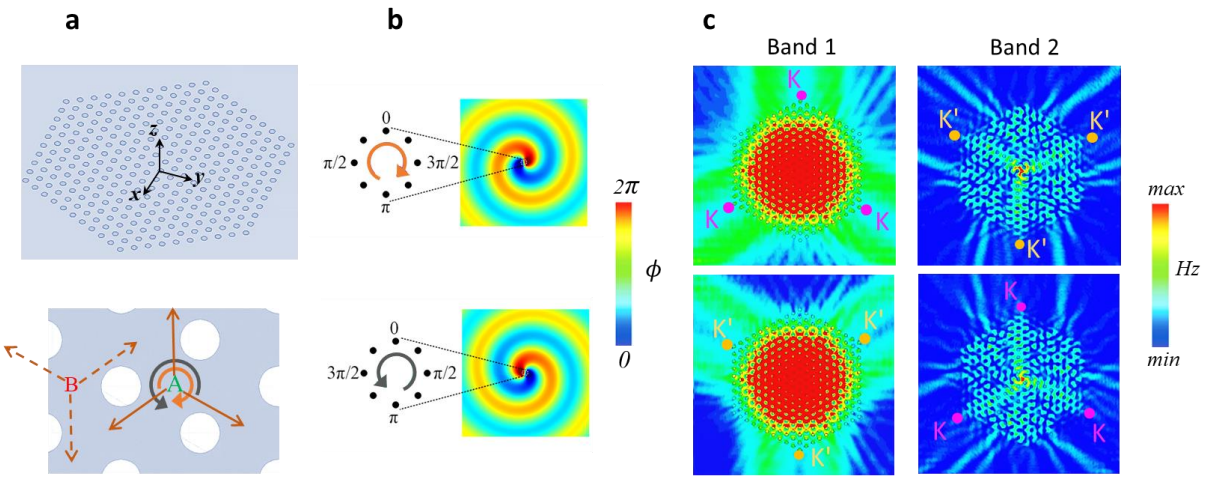

Figure 2. (a) A triangular-lattice PhC of a finite size with a hexagonal-shaped area, over which the fields in Fig. 2c are plotted. At the center of the PhC is the OAM excitation source, which is comprised of an arrangement of Hz dipole-point sources with same magnitudes but incrementally increasing phases in rotational manner as shown in (b). (c) Surface plot of electric-field intensity showing valley-contrasting response; modes propagate along either K or K′ when excited at the center by an OAM source, depending on whether the source has clockwise (cw) or counterclockwise (ccw) phase rotation, respectively. This observation holds for both first and second bands surrounding the bandgap but with the modes locked to opposite directions like in typical valley PTI structures.

When operating at frequency at the extrema of band 1 and having the phases of H_z sources increase clockwise (top panel of Fig. 2b), waves propagate towards only three corners (namely, upper-most, lower-left and lower-right) and not all six corners of the hexagonal PhC region. These directions correspond to the K point in momentum space, which means that the clockwise OAM polarity locally defines the K valley-polarized state. In contrast, when counter-clockwise OAM source is used at the same frequency, wave propagation flows to the opposite direction, indicating that counter-clockwise OAM polarity is locked to the K′ valley. Meanwhile, the opposite response is observed for band 2 at the K and K′ valleys (right panels of Fig. 2b), i.e. counter-clockwise/clockwise OAM states locally define the K/K′ valley polarization, respectively. Such distinct differences in wave propagation directions and the phase distributions

prove that an ordinary triangular-lattice PhC supports valley-contrasting response in an analogous manner to conventional QVH PTI. Unlike QVH PTI, however, these polarization states are not uniquely defined throughout the bulk. For example, the valley polarizations will switch when the excitation source is placed at position B in the bulk as depicted in the lower panel of Fig. 2a.

Valley polarized edge modes:

Robust edge states in a system with an insulating bulk are often related to topological order and are the main reason for the great interest in investigating and realizing PTIs. Valley polarized edge states appear in QVH PTIs, where a bulk bandgap is opened by SIS breaking (analogous to their condensed matter counterparts, for instance, in AB stacked and electrically biased bilayer graphene). By breaking the SIS of the unit cell, either through altering the size of A and B atoms in honeycomb lattice or through using triangular shaped atoms in triangular-lattice PhC, a controllable bandgap separating different topological phases of guided modes can be achieved. In contrast, the bandgap in our PhC is not the result of SIS breaking, hence it is unexpected that similar protected edge states to appear in this bandgap. In the following we describe how to exploit the local VHE to realize such states.

The QVH effect manifests itself in valley polarized edge states that occur at the domain walls between, for example, AB and BA-stacked electrically biased bilayer graphene [25–27], where the topological valley phases are different. In fact, the conservation of the binary valley DOF is responsible for the topologically protected edge states despite the absence of genuine Chern number; the Berry curvature integration must be restricted to half of the BZ associated with the

K (K′) valley. The bulk-boundary correspondence principle prohibits topological edge states at the interface between a valley-projected topological phase and a topologically trivial phase. However, the domain wall between valley crystals with half-integer valley-Chern numbers of the opposite sign allow for edge states (also referred to as kink states). Hence, these states are a consequence of separate domains with opposite spontaneous orbital moments. [25]

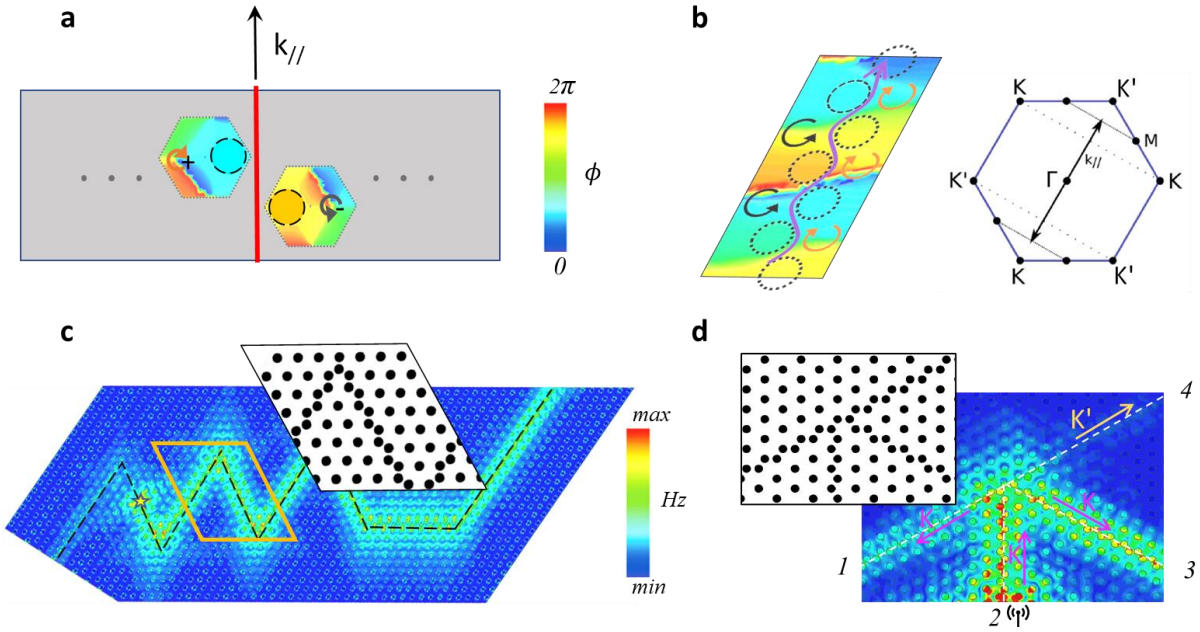

Figure 3. (a) Surface field map of Hz phase within unit cells with off-center air hole, showing singular phase points with opposite senses of phase rotation (i.e. sign of OAM) depending on the location of the air hole relative to the unit cell's center. (b) Surface distribution map of Hz phase at the interface between two lattices with opposite shifts in air hole positions. The interface supports a localize mode, whose propagation direction is defined by the relative orientation of the opposite OAM polarities (equivalently, energy flux vortexes) on the two sides. (c) Simulated surface field map of E-field intensity over the complete proposed PhC waveguide, showing unidirectional excitation of the edge mode when using an OAM source (denoted by yellow star), energy localization near the topological interface (marked by dashed black line) and reflection-immune wave transmission along a meandering pathway. The inset shows the holes arrangement at a zigzag section of the waveguide. (d) planar magic-T junction showing valley polarization states routing, each polarization state towards its corresponding valley direction analogous to spin-momentum locking.

Where only a local region is concerned, as is the case for waveguide scenario, the local VHE upholds valley DOF. As Fig. 3a shows, shifting the air hole off-center to the right half of the unit cell of our triangular PhC is accompanied by a phase singular point appearing to the left, which carries a clockwise (counter-clockwise) OAM at the K valley of the first (second) band. In contrast, shifting the air hole off-center to the left half of the unit cell is accompanied by a phase singular point appearing to the right, which carries a counter-clockwise (clockwise) OAM at the same valley of the first (second) band. Importantly, the reversal of frequency order (first/second bands) of the OAM states at each valley as the air hole position moves past the center of the unit cell is like to that in the QVH PTIs with a topological phase transition. Accordingly, we can interface the two lattices, which have inverted air holes positions with respect to each other to create a defect line-like interface. Note that the two lattices are interfaces such that the translation symmetry is preserved along the direction parallel to interface (denoted by $k_{//}$ in the Fig. 3a and Fig. 3b). That is, the interface is aligned with the ΓK and ΓK′ directions of the PhC. Meanwhile, far from the interface region, the PhCs on the two sides appear identical (see inset of Fig. 3c).

Fig. 3b shows simulated surface field map over a zoom-in region of the interface, which exhibits opposite OAM polarities on the two respective sides as indicated by the curled arrow directions. When operating at a frequency within the bandgap between first and second bands of the PhC, the phase discontinuity in the electromagnetic fields' distribution across the interface, in the form of canceling OAMs (i.e. have opposite signs), leads to field localization and the occurrence of valley edge modes. Since the PhC bandgap is in the guide part of the band diagram (i.e. below the light line), the fields of the edge modes will be confined in the plane of the PhC slab. In addition, a linkage between the propagation direction (here along $k_{//}$, noted in the BZ illustration of Fig. 3b) and the specific signs of the OAM polarities across the interface gives rise to

direction-locked propagation, meaning the edge modes are valley polarized. For example, the depicted OAM polarities in Fig. 3b are associated with upward propagating mode, as indicated by the magenta-colored wavy arrow along the defect line interface. Since the band diagram is symmetric with respect to the wavevector, there exists a pair of counter-propagating edge states with opposite valley-polarizations. These states are uncoupled from each other in the absence of inter-valley scattering.

To demonstrate the robustness of the proposed edge modes, we tested waveguides featuring multiple sharp turns and utilized an RCP source (schematically shown as star in Fig. 3c) to launch the edge mode with K-valley polarized state at a frequency within the PhC bandgap. The field intensity map over the surface of the entire PhC area shows that the edge mode is transmitted unidirectionally to the right of the sample. Furthermore, the fields are concentrated near the interface (marked as dashed black line) and the wave propagates through every bent segment without reflection. In case of valley PTI as well as our PhC, only zigzag-shaped pathway along ΓK inclination, which conserve the valley DOF, could support robust valley-polarized edge states. Except for perturbations that alter the C_{3v} symmetry, intervalley scattering is well suppressed by the large momentum separation of K and K′ points [12].

We further prove the nature of the edge modes of our defect line waveguide and the reason for their robustness by testing the wave routing through the planar magic-T junction depicted in Fig. 3d. There are four interfaces (domain walls) separating lattices with shifted unit cell center (inverted relative air hole position, as shown in the inset). All the interfaces, which support valley edge states, intersect at one point. The simulated surface field distribution show that when wave is injected from port 2 at a frequency within the bulk bandgap, it is routed into ports 1 and

3 but not port 4. Counterintuitively, this happens even though the deflection angles from port 2 to ports 1 and 3 are much larger than that from port 2 to port 4. This is due to the propagation direction of the edge mode being naturally locked to its valley polarization. As marked in Fig. 3d, the guided mode in the input port 1 belong to the K valley, which is of the same valley polarization of the output ports 1 and 3. The valley polarization of the output port 4, however, belongs to the K′ valley, so light cannot be coupled efficiently into this port owing to conservation of the valley DOF. As such, the edge states in our PhC indeed share the same origin as the VHE and inherit similar features to topological edge states in QVH PTIs. Therefore, as far as robustness against sharp bends is concerned, there is virtually no difference between the capability of our defect line PhC waveguide and topological valley PhC waveguides.

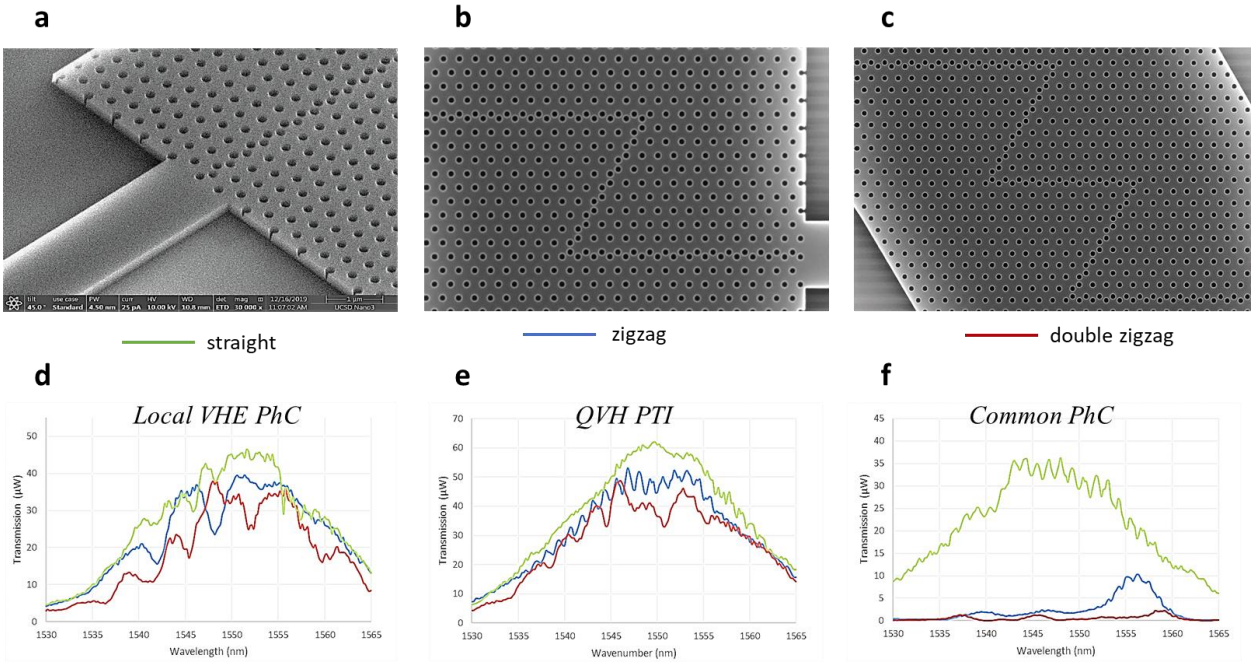

Figure 4. (a, b, c) Top-view scanning-electron-microscope images of the fabricated samples, including straight, zigzag and double zigzag interfaces, respectively. The zigzag shape interface with two (four) 120o bends shows that light can smoothly propagate around the corners. (d, e, f) Measured transmission spectra along the different pathways in the proposed local VHE PhC, a conventional QVH PTI and common defect line PhC waveguide, respectively. Only in case of the local VHE PhC and QVH PTI, the

spectra in the bandgap maintain the flat-top high transmittance, even for a sharp-bending geometry. This intriguing property indicates broadband robust transport.

Optical Measurements:

To experimentally demonstrate robust transport of the valley-polarized edge states, we fabricate waveguide devices with straight, zigzag, and double zigzag interfaces. All waveguides are built using standard SOI wafer, where the slab is made of silicon, Si, with a relative permittivity of 11.9 and the substrate is made of silica, SiO_2, with a relative permittivity of 4. We chose a lattice constant of 420 nm, diameter of the air hole of 180 nm and thickness of the slab of 220 nm. The devices were covered with 2μm buried oxide layer. This gives TE bandgap spanning the wavelengths range 1460nm to 1640nm. The scanning-electron-microscope (SEM) images of fabricated samples are shown in Fig. 4a–c. To measure the transmission spectra of the fabricated devices, light from a tunable semiconductor laser was coupled via a single-mode fiber to the SOI PhC waveguides through an integrated grating coupler, which has a 3-dB bandwidth of ≈ 35 nm. The TE-polarized continuous waves at the telecommunication wavelength were coupled to a 1.7μm-width input rectangular waveguide then launched into the PhC sample. After passing through the PhC, the propagating wave was coupled to the output rectangular waveguide then collected by another grating coupler. The corresponding transmission spectra were detected by an optical powermeter, with tuning the operation wavelength of excited waves.

Fig. 4d shows the measured transmission spectra in the wavelength range of 1530–1565nm, for straight, zigzag, and double zigzag interfaces of the proposed local VHE PhC waveguide. In the bandgap region, the spectra show high transmittance comparable for the three interfaces. This

insensitivity to sharp bends indicates suppression of intervalley scattering. For reference, similar waveguide devices using a typical QVH PTI [20] were fabricated and tested. The measured transmission spectra, plotted in Fig. 4e, are found comparable to the results from the waveguides of the local VHE PhC. In addition, we fabricate and test a typical defect line PhC waveguide [28] along similar sharp bends. As shown in Fig. 4f, light transmission is greatly deteriorated due the sharp bends in contrast to the previous two group of devices, as expected.

Conclusion:

We have demonstrated a new approach for realizing valley-polarized edge modes and experimentally confirmed their robust light transmission through sharp bends using a silicon-on-insulator (SOI) slab at telecommunication wavelengths. These modes share the same origin as the VHE and inherit similar feature to topological edge states in QVH PTIs although are implemented on a common triangular PhC with no topological order. This is done by rearranging one row of air holes like in common line defect waveguides such that opposite OAM states are enforced near the two sides of the waveguide region. Despite its simplicity and the widespread use of defect line waveguides in triangular PhCs, this effect has until now eluded observation. Our results present a new perspective to the existence of gapless chiral edge states and open new avenues to develop compact on-chip optical devices with low loss, such as compact delay lines, on-chip isolation, slow-light optical buffers, and lasers. Lastly, while our demonstration concerns photonic systems, the local VHE, which can be regarded as a generalization of the VHE, is applicable to other wave systems such as plasmonics, mechanics and acoustics.

Acknowledgements

This work was supported in part by DARPA contract W911NF-17-1-0580.

Conflict of Interest

The authors declare no conflict of interest.